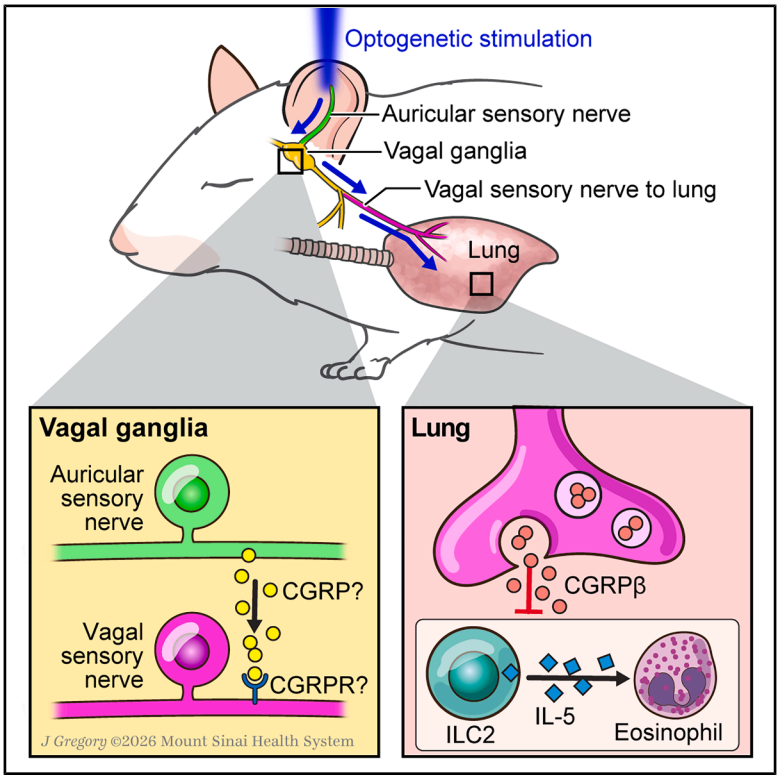
Report

Immunity

Activation of the auricular vagus nerve reflex suppresses airway inflammation

Graphical abstract



Authors

Rintaro Shibuya, Nobuya Abe, Keaton Song, ..., Kenji Kabashima, Hongzhen Hu, Brian S. Kim

Correspondence

bkim26@northwell.edu

In brief

Bioelectronic technologies are being deployed to treat many inflammatory conditions using transcutaneous auricular nerve stimulation. Shibuya et al. employ viral tracing, chemogenetics, and optogenetics to unveil a sensory skin-lung vagal reflex that suppresses allergic airway inflammation. They identify the neuropeptide CGRPβ as a key mediator and provide a rationale for transcutaneous bioelectronic neuromodulation in asthma.

Highlights

- Auricular skin contains TRPV1^{+} vagal sensory afferents
- Activation of these afferents suppresses allergic airway inflammation
- Vagal afferent-derived CGRPβ is necessary to suppress lung inflammation
- Auricular vagus nerve stimulation may represent a therapeutic modality

Shibuya et al., 2026, Immunity 59, 2402–2412
September 8, 2026 © 2026 The Authors. Published by Elsevier Inc.
https://doi.org/10.1016/j.immuni.2026.06.005

CellPress

CellPress
OPEN ACCESS

Immunity

Report

Activation of the auricular vagus nerve reflex suppresses airway inflammation

Rintaro Shibuya,[1,2,3,4,5,6,7] Nobuya Abe,[1,3,5,6,8] Keaton Song,[1,3,4,5,6,8] Nathan D. Rossen,[1,2,3,4,5,6] Masato Tamari,[9] Zhen Wang,[1,2,3,4,5,6] Zili Xie,[1,3,5,6,11] Yuki Abe,[1,3,5,6,8] Hisato Iriki,[10] Ayana Iijima,[1,2,3,4,5,6] Lydia Zamidar,[1,2,3,4,5,6] Xu Li,[1,2,3,4,5,6] Xia Meng,[1,2,3,4,5,6] Andras Bimbo-Szuhai,[4] Veronica Burstein,[1,3,4,5] Jill K. Gregory,[11] Natalia P. Biscola,[1,2,3,4,5,6] Karen Anthony,[1,2,3,4,5,6] Michel Enamorado,[1,3,4,5] Steven J. Van Dyken,[12] Kenji Kabashima,[7,13] Hongzhen Hu,[1,3,5,6,8] and Brian S. Kim[1,2,3,4,5,6,14,15,*]

[1]Kimberly and Eric J. Waldman Department of Dermatology, Icahn School of Medicine at Mount Sinai, New York, NY 10029, USA
[2]Department of Immunology and Immunotherapy, Icahn School of Medicine at Mount Sinai, New York, NY 10029, USA
[3]Mark Lebwohl Center for Neuroinflammation and Sensation, Icahn School of Medicine at Mount Sinai, New York, NY 10029, USA
[4]Marc and Jennifer Lipschultz Precision Immunology Institute, Icahn School of Medicine at Mount Sinai, New York, NY 10029, USA
[5]Friedman Brain Institute, Icahn School of Medicine at Mount Sinai, New York, NY 10029, USA
[6]Allen Discovery Center for Neuroimmune Interactions, Icahn School of Medicine at Mount Sinai, New York, NY 10019, USA
[7]Department of Dermatology, Kyoto University Graduate School of Medicine, Sakyo-ku, Kyoto 606-8507, Japan
[8]Nash Family Department of Neuroscience, Icahn School of Medicine at Mount Sinai, New York, NY 10029, USA
[9]Allergy Center, National Center for Child Health and Development, Setagaya-ku, Tokyo 157-8535, Japan
[10]Laboratory for Skin Homeostasis, RIKEN Center for Integrative Medical Sciences, Yokohama, Kanagawa 230-0045, Japan
[11]Digital and Technology Partners, Icahn School of Medicine at Mount Sinai, New York, NY 10029, USA
[12]Department of Pathology and Immunology, Washington University School of Medicine, St. Louis, MO 63110, USA
[13]Singapore Immunology Network and Skin Research Institute of Singapore, Agency for Science, Technology and Research (A*STAR), Singapore 308232, Singapore
[14]Lead contact
[15]Present address: Laboratory of Neuroimmunology, Feinstein Institutes for Medical Research, Northwell Health, Manhasset, NY, 11030, USA.
*Correspondence: bkim26@northwell.edu
https://doi.org/10.1016/j.immuni.2026.06.005

SUMMARY

The vagus nerve regulates inflammation via sensory-motor arcs. While vagal sensory neurons relay signals from within the body (interoception), whether external inputs can regulate visceral neuroimmune responses (exteroception) remains poorly understood. We unveiled a skin-lung reflex by which sensory neurons from the auricular skin suppressed *Alternaria alternata*-induced allergic airway inflammation. Viral and chemical neural tracing revealed distinct sensory projections from the vagal ganglia to the auricular skin. Pharmacologic, chemogenetic, and optogenetic activation of auricular transient receptor potential vanilloid 1 (TRPV1)$^+$ afferents attenuated type 2 allergic lung inflammation, including group 2 innate lymphoid cell, eosinophil, and type 2 cytokine responses in the airway. Conversely, silencing of these sensory neurons via the skin exacerbated lung inflammation, and immunosuppression of airway inflammation was dependent on the neuropeptide calcitonin gene-related peptide (CGRP)β. These findings reveal an evolutionarily conserved somato-visceral reflex by which exteroceptive inputs impact visceral inflammation. Thus, transcutaneous neuromodulation may represent a therapeutic strategy to treat visceral inflammation.

INTRODUCTION

Neuroimmunology has emerged as a major field of metabiology that reveals previously underappreciated processes at the organismal level.[1] Sensory neurons, upon depolarization, transmit action potentials to relay sensation to the central nervous system (CNS). However, in response to stimuli, they also shape immune, stromal, and epithelial responses across tissues and disease states. These efferent functions are mediated by the release of neuropeptides such as calcitonin gene-related peptide (CGRP) and substance P.[2–5] This integration of sensation and neuroinflammation has redefined our understanding of how sensory neurons impact inflammation, infection, and tissue homeostasis.[2–15]

The vagus nerve is a master regulator of systemic immune responses, in part, through the cholinergic anti-inflammatory pathway (CAP).[16–18] Leveraging this biology, the first vagus nerve stimulator (VNS) was recently FDA-approved for difficult-to-treat rheumatoid arthritis (RA).[19] Thus, bioelectronic medicine has emerged as a unique field in which devices are used to

This is an open access article under the CC BY-NC license (http://creativecommons.org/licenses/by-nc/4.0/).

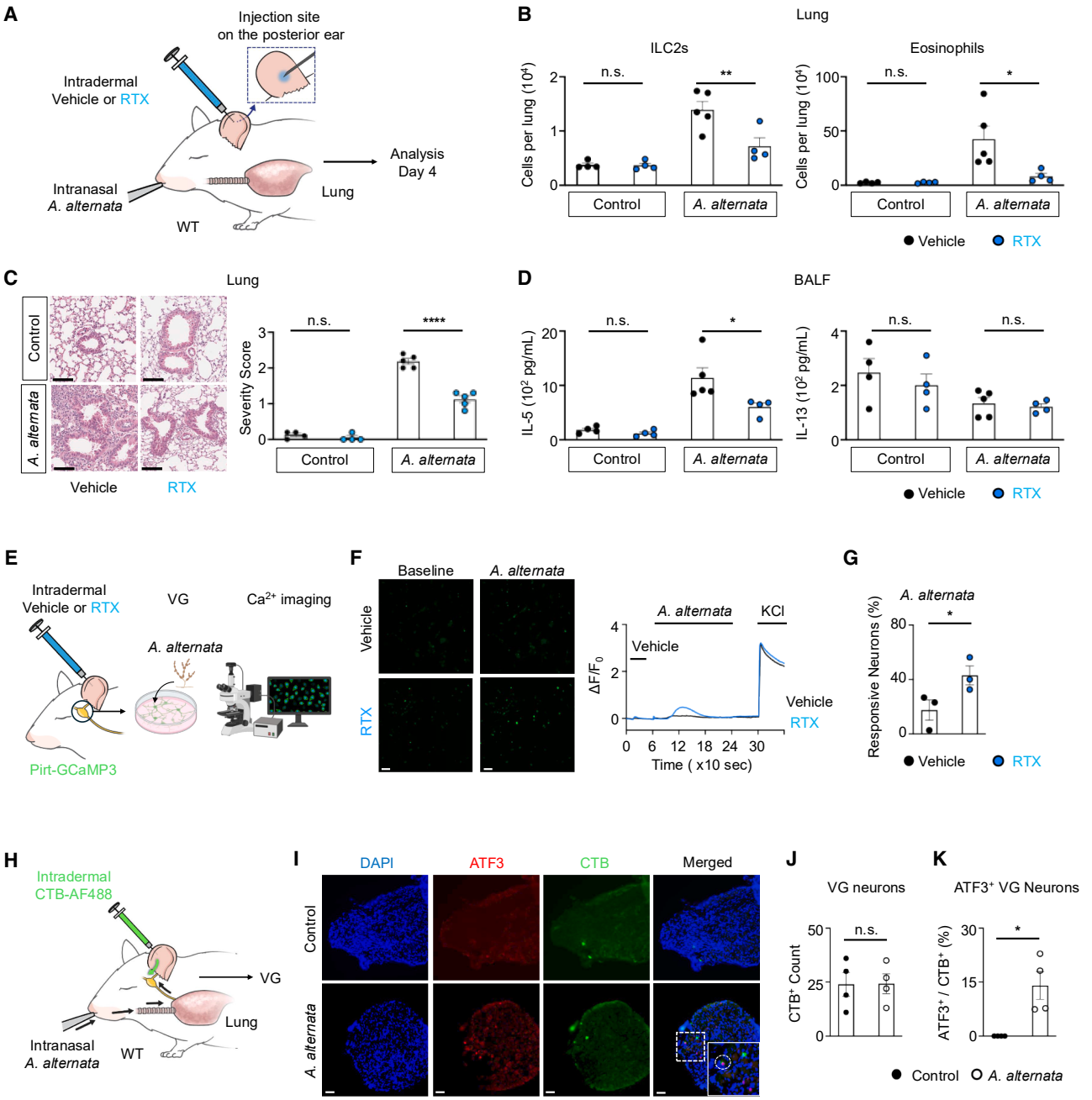


Figure 1. TRPV1 activation in the skin suppresses allergic airway inflammation

(A) Wild-type (WT) mice received i.d. RTX (100 ng/ear) or vehicle in the central dorsal aspect of the auricle on day 0, followed by intranasal *A. alternata* (2 μg) or no treatment on days 0–3. Lung and bronchoalveolar lavage fluid (BALF) samples were harvested and analyzed on day 4.

(B) Quantification of lung ILC2 and eosinophil numbers by flow cytometry.

(C) Representative lung histology (H&E) with severity scores. Scale bars, 100 μm.

(D) BALF IL-5 and IL-13 proteins measured by ELISA. Data are representative of two independent experiments (n = 4–5 mice/group).

(E) Pirt-GCaMP3 mice received i.d. RTX or vehicle on day 0. Vagal ganglia (VGs) were harvested on day 4, cultured for 3 days, and imaged on day 7. Cultured cells were challenged with vehicle (ACSF) at 15 s, *A. alternata* (10 μg/mL) at 60 s, and KCl at 300 s.

(F) Representative field and mean traces. Scale bars, 50 μm.

(G) Percentage of *A. alternata*-responsive neurons among KCl-responsive neurons. Results are representative of two independent experiments (n = 3 mice/group).

(H) WT mice received i.d. CTB-AF488 (5 μg/ear) on day 0 and intranasal *A. alternata* or PBS on days 0–3. VGs were collected on day 4.

(I) Representative VG images showing ATF3 and the auricular tracer CTB-AF488. Scale bars, 50 μm.

(legend continued on next page)

electronically manipulate neural circuits to treat a myriad of inflammatory disorders. Given the expansive anatomic network of the vagus nerve, the ways in which this organ can be modulated remain a field of inquiry.

A small projection of the vagus nerve, known as the auricular branch, is the only known component to innervate a somatosensory organ, namely the skin.[20,21] The functions of this small branch remain unclear. Notwithstanding this, transcutaneous VNS, targeting the auricular branch, has garnered attention for its ability to noninvasively modulate the vagus nerve.[21–24] Understanding how bioelectronic neuromodulation functions in the skin may expand avenues of neuroimmune therapy.

In the setting of allergic lung inflammation, we showed that vagal neurons that innervate the skin become stimulated. Local activation of transient receptor potential vanilloid 1 (TRPV1)-positive sensory afferents in the skin suppressed airway inflammation. Chemogenetic or optogenetic stimulation of auricular TRPV1$^+$ fibers increased airway CGRPβ protein to attenuate lung inflammation. Conversely, chemogenetic inhibition of these fibers exacerbated airway disease. Our findings uncover a skin-lung vagal sensory reflex arc that regulates allergic lung inflammation.

RESULTS

TRPV1 activation in the skin suppresses allergic airway inflammation

The auricular branch of the vagus nerve courses along the external ear (auricle), but its precise anatomic distribution remains poorly defined.[20–22] To map nerves from the skin to the vagal ganglion (VG), we introduced a retrograde adeno-associated virus (AAV) expressing Cre recombinase into the auricular skin of *Rosa26*$^{LSL\text{-}tdTomato}$ mice (Figure S1A). In these mice, we could identify a population of tdTomato$^+$ neurons in the VG, confirming direct skin innervation (Figure S1B). As expected, we also observed labeling of neurons within the corresponding dorsal root ganglia (DRGs) but not the trigeminal ganglia (TGs). Thus, the auricular skin receives sensory input from both the VG and the DRG.

To test the specificity of VG innervation to the auricular skin, we injected AAV9-Cre into the VG of *Rosa26*$^{LSL\text{-}tdTomato}$ mice (Figure S1C). This approach only labeled fibers in the auricular skin but not in the cheek skin (Figure S1D). Conversely, AAV9-Cre delivery to the VG did not result in labeling of DRG or TG, indicating that injections of virus into the VG do not leak into neighboring ganglia that project to the skin (Figures S1E and S1F). To orthogonally interrogate the identity of these vagal afferents, we injected a fluorescently conjugated Alexa Fluor 647-wheat germ agglutinin (WGA-AF647) into the VG to label skin-projecting nerves (Figure S1G). The AF647$^+$ fibers we observed in the auricular skin were CGRP$^+$, indicating their sensory and peptidergic identity (Figure S1H). To examine the distribution of VG-derived fibers in the auricular skin relative to spinal DRG afferents, we performed dual WGA-based tracing (Figure S1I). Indeed, DRG-derived sensory nerve fibers were also detected within the auricular skin (Figures S1J–S1K).

We and others have shown that the lung is almost exclusively innervated by VG.[3,25] Thus, we hypothesized that lung inflammation could be influenced by auricular stimulation. To test this, we used a previously established model of allergic lung inflammation induced by the protease allergen *Alternaria alternata* (*A. alternata*).[26–28] We employed intradermal (i.d.) injection of resiniferatoxin (RTX), a potent agonist of TRPV1, into the auricle. While at high doses RTX causes depolarization of TRPV1$^+$ neurons and denervation,[29,30] at low doses it causes near-term activation.[31] Upon i.d. injection, mice were exposed to *A. alternata* intranasally for 4 days (Figure 1A). While RTX alone did not alter the composition of type 2 immune cells in the lung at steady state (Figures 1B and S1L), it suppressed type 2 inflammation in the setting of *A. alternata* exposure (Figure 1B). Histopathology was also improved in terms of inflammatory infiltrates (Figure 1C), and interleukin (IL)-5 was significantly reduced following RTX treatment (Figure 1D). These results indicate that cutaneous TRPV1$^+$ sensory neurons suppress allergic airway inflammation.

To investigate whether this interorgan regulation is accompanied by vagal neuron activation, we performed Ca^{2+} imaging of VG neurons from Pirt-GCaMP3 mice in which the genetically encoded calcium indicator GCaMP3 is driven by the sensory neuron-specific *Pirt* promoter. Studies have shown that *A. alternata* can directly trigger Ca^{2+} responses in DRG neurons.[2,32] We found that *A. alternata* evoked larger Ca^{2+} transients in VG neurons from RTX-treated mice than those from controls (Figures 1E, 1F, and S1M). Potassium chloride (KCl) evoked similar responses in both groups, suggesting that cellular viability and membrane excitability were preserved regardless of RTX exposure (Figure S1M). Moreover, the fraction of *A. alternata*-responsive neurons among KCl-responsive neurons was significantly increased in VG neurons from RTX-treated mice (Figure 1G). These results reveal that auricular stimulation enhances vagal sensory neuron responsiveness to *A. alternata*. To test whether neural hypersensitivity elicited by RTX was restricted only to afferent neurons supplying the lung, cholera toxin B (CTB)-AF647 was delivered into the airway, and allergen-evoked Ca^{2+} responses were compared between CTB$^+$ and CTB$^-$ VG neurons *ex vivo* (Figure S1N). Enhancement of Ca^{2+} responses extended beyond lung-traced CTB$^+$ neurons (Figure S1O).

We next asked whether allergic lung inflammation can enhance the responsiveness of VG neurons that specifically innervate the skin. To test this, CTB-AF488 was injected i.d. to label skin-innervating VG neurons. We then compared mice that were treated with *A. alternata* to control mice, and VGs were analyzed by immunofluorescence (Figure 1H). We observed similar numbers of CTB$^+$ skin-innervating neurons from *A. alternata*-treated mice compared with controls (Figure 1J). However, CTB$^+$ neurons that were exposed to

(J) CTB$^+$ cells per VG.

(K) Percentage of ATF3$^+$ neurons among CTB$^+$ neurons. Results are representative of two independent experiments (n = 4 VGs/group).

Mean ± SEM; two-way ANOVA followed by Bonferroni's multiple comparisons test (B–D) and unpaired t test with Welch's correction (G, J, and K). *$p < 0.05$, **$p < 0.01$, ****$p < 0.0001$, not significant (n.s.).

See also Figures S1–S3.

A. alternata in the airway exhibited increased expression of ATF3, a marker associated with neuronal stress/injury and activation (Figure 1K).[14,33–35,36] In addition to labeling VG neurons from the skin with CTB-AF488, we also labeled VG neurons from the lung separately using CTB-AF647 (Figure S2A). Dual retrograde tracing revealed that skin- and lung-associated neurons were distinctly localized within the VG (Figure S2B). However, we found a number of skin- and lung-derived neurons that were in close proximity to one another (Figure S2B). Collectively, these anatomical, physiological, and immunologic findings support a functional linkage between skin- and lung-associated vagal fibers.

RTX selectively activates TRPV1$^+$ sensory (i.e., afferent) neurons. However, it is possible that local activation of the auricular nerve by RTX is dependent on autonomic (i.e., efferent) neurons to influence lung inflammation. To test this, we first delivered 6-hydroxydopamine (6-OHDA) to chemically denervate sympathetic neurons during allergic lung inflammation (Figure S3A). In this context, RTX-mediated immunosuppression was unaffected by chemical sympathectomy (Figure S3B). Conversely, we separately delivered glycopyrrolate or mecamylamine to block muscarinic and nicotinic acetylcholine receptors, respectively, in the setting of lung inflammation (Figures S3C and S3E). Disruption of parasympathetic signaling did not affect the capacity of i.d. RTX to suppress lung inflammation (Figures S3D and S3F). Taken together, autonomic output appeared to be dispensable in mediating this anti-inflammatory reflex.

Chemogenetic manipulation of vagal TRPV1$^+$ neurons in the auricular skin regulates allergic airway inflammation

We next undertook an orthogonal approach to test whether chemogenetic activation of TRPV1$^+$ nerve fibers would also recapitulate a skin-lung neuroimmune circuit. We crossed *Trpv1*^{Cre} with *Rosa26*$^{LSL\text{-}hM3Dq}$ mice to generate *Trpv1*^{hM3Dq} mice, in which expression of a Gq-coupled designer receptor (DREADD) permits selective activation of TRPV1$^+$ neurons with clozapine N-oxide (CNO).[37,38] *Trpv1*^{hM3Dq} or *Rosa26*$^{LSL\text{-}hM3Dq}$ control mice received i.d. CNO into the auricular skin followed by exposure to *A. alternata* (Figure S4A). Flow cytometry revealed a significant reduction in group 2 innate lymphoid cell (ILC2) and eosinophil numbers in *Trpv1*^{hM3Dq} mice compared with control mice during allergic lung inflammation (Figure S4B). Accordingly, *Trpv1*^{hM3Dq} mice exhibited an improvement of lung pathology (Figure S4C) in association with reduced ILC2-derived IL-5 and IL-13 and lower IL-5 protein in the bronchoalveolar lavage fluid (BALF) (Figures S4D and S4E). These results further support the importance of skin-innervating TRPV1$^+$ afferents as a key suppressor of allergic lung inflammation.

Neuropeptides released from sensory neurons such as CGRP or substance P are known to regulate inflammation.[3,8,39–41] We thus hypothesized that they could be involved in the auricular-vagal circuit. We measured CGRPα, CGRPβ, and substance P in BALF from *Trpv1*^{hM3Dq} and control mice that received i.d. CNO and intranasal *A. alternata* (Figure S4A). There was no difference in CGRPα or substance P observed in both groups (Figure S4F). By contrast, CGRPβ protein was significantly elevated in *Trpv1*^{hM3Dq} mice (Figure S4F). These data suggest that activation of TRPV1$^+$ afferents in the auricular skin selectively enhances CGRPβ production in the airway.

We next sought to manipulate TRPV1$^+$ neurons in the skin that exclusively arise from the VG. To this end, we inserted Gq DREADD into TRPV1$^+$ neurons arising from the VG via intravagal injection of AAV. To do so, we injected AAV9-hSyn-DIO-hM3Dq-mCherry (double-floxed inverted open reading frame [DIO]) or control AAV into the VG of *Trpv1*^{Cre} mice. Recipient mice received i.d. CNO and intranasal *A. alternata* (Figure 2A), and mCherry$^+$ fibers were visualized in the auricle, confirming viral payload delivery (Figure S4G). All parameters of inflammation were reduced as measured by flow cytometry, histology, and cytokine production (Figures 2B–2E). Notably, CGRPβ protein was increased in BALF (Figure 2F). These results demonstrate that skin activation of bona fide TRPV1$^+$ vagal afferents suppresses lung inflammation.

Conversely, we sought to determine whether inhibition of cutaneous TRPV1$^+$ neurons would aggravate lung inflammation. We thus generated *TRPV1*^{hM4Di} mice expressing an inhibitory DREADD and subjected them to i.d. CNO in the setting of *A. alternata* exposure (Figure S4H). All parameters of inflammation were aggravated in *TRPV1*^{hM4Di} mice (Figures S4I–S4L) in association with reduced CGRPβ protein in BALF (Figure S4M). To specifically manipulate VG-derived TRPV1$^+$ neurons in the skin, we injected AAV9-hSyn-DIO-hM4Di-mCherry into the VG of *Trpv1*^{Cre} mice. Recipient mice received i.d. CNO and *A. alternata* (Figure 2G), and mCherry$^+$ fibers were visualized in the auricle (Figure S4N). All parameters of inflammation were increased (Figures 2H–2K) in association with reduced CGRPβ protein in BALF (Figure 2L). Collectively, these results demonstrate that, in contrast to activation, inhibition of skin TRPV1$^+$ vagal afferents aggravates airway inflammation.

Deletion of *Calcb* in vagal sensory neurons disrupts the skin-lung neuroimmune circuit

To test the precise role of CGRPβ as an effector neuropeptide, we injected AAV-Cre into the VG of *Calcb*$^{fl/fl}$ (*Calcb*$^{\Delta VG}$) mice to selectively delete *Calcb*, which encodes CGRPβ. *Calcb*$^{\Delta VG}$ mice received i.d. RTX to the auricular skin together with intranasal *A. alternata* (Figure 3A). qPCR of VG demonstrated reduced *Calcb* mRNA expression in conjunction with reduced CGRPβ protein (Figures 3B and 3C). In parallel, lungs from *Calcb*$^{\Delta VG}$ mice showed more pronounced parameters of inflammation (Figures 3D–3G). To undertake a therapeutic proof-of-concept approach, we treated wild-type mice with the CGRP receptor antagonist BIBN4096 following i.d. RTX and *A. alternata* challenge (Figure 3H). BIBN4096 reversed the anti-inflammatory effects of RTX in the lungs (Figures 3I–3L); however, it did not alter CGRPβ protein in BALF (Figure 3M). These findings demonstrate that CGRPβ is a key downstream effector of the skin-lung circuit.

Optogenetic stimulation of the auricular branch of the vagus nerve in the skin suppresses allergic airway inflammation

To more closely mimic transcutaneous VNS, as currently being explored therapeutically, we undertook an optogenetic approach using channelrhodopsin-2 (ChR2).[42,43] ChR2-based photostimulation confines activation only to light-exposed skin, thereby providing highly localized activation of cutaneous vagal sensory neurons with no systemic exposure. We then delivered a

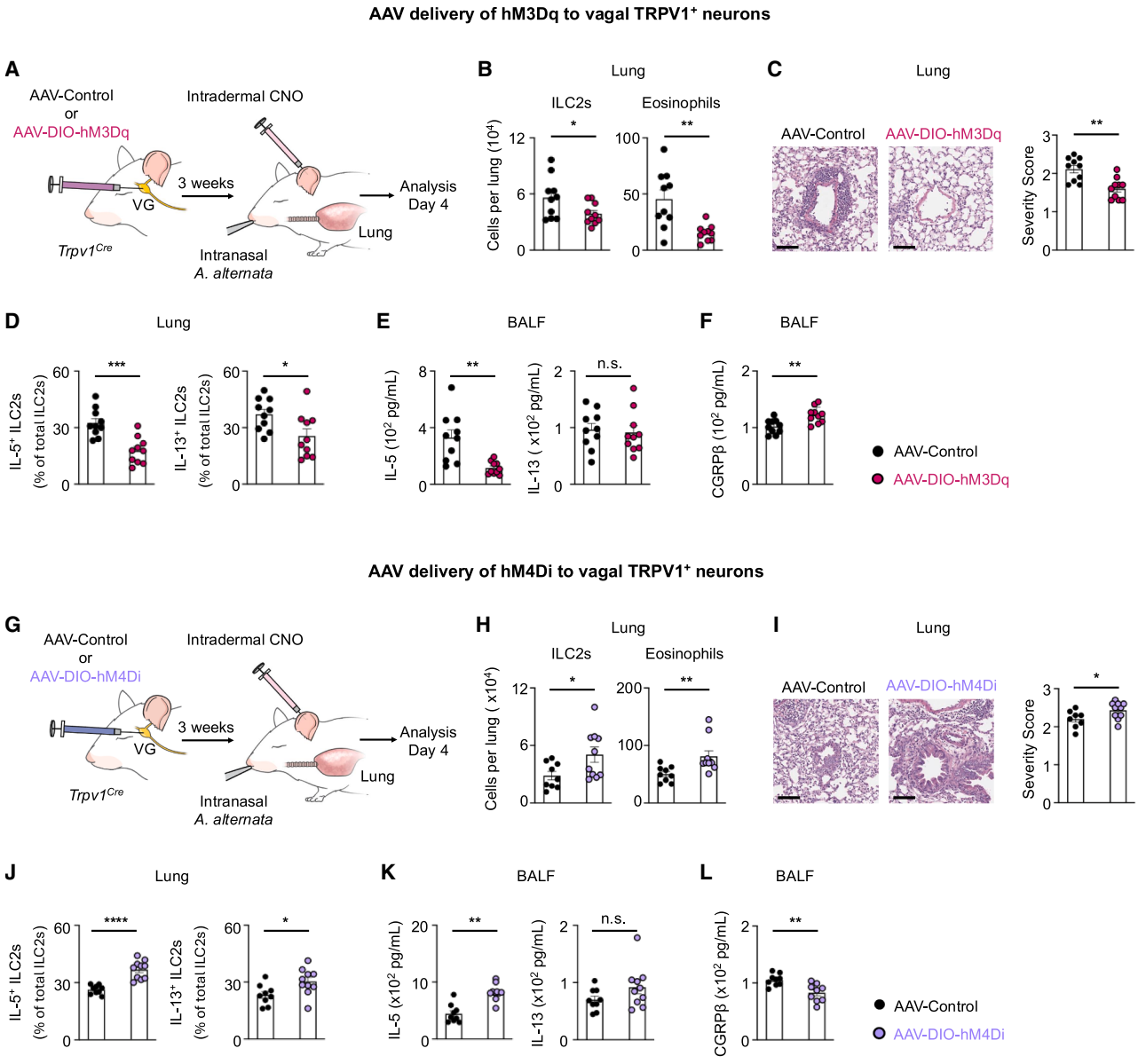


Figure 2. Chemogenetic manipulation of vagal TRPV1⁺ neurons in the auricular skin regulates allergic airway inflammation

(A) *Trpv1*^{Cre} mice received an intraganglionic injection with AAV9-DIO-hM3Dq-mCherry or AAV9-DIO-mCherry (AAV-Control) in the VG. 3 weeks after injection, mice received once-daily i.d. CNO (0.05 mg/kg) in the dorsal auricle plus intranasal *A. alternata* on days 0–3 and were analyzed on day 4.

(B) Lung ILC2 and eosinophil numbers by flow cytometry.

(C) H&E histology and severity scores. Scale bars, 100 μm.

(D) ILC2 cytokine production after phorbol 12-myristate 13-acetate (PMA)/ionomycin stimulation.

(E) IL-5 and IL-13 proteins in BALF.

(F) CGRPβ protein in BALF. Data are pooled from two independent experiments (n = 10 mice/group).

(G) *Trpv1*^{Cre} mice received an intraganglionic injection with AAV9-DIO-hM4Di-mCherry or AAV-Control into the VG. 3 weeks later, mice received i.d. CNO and intranasal *A. alternata* on days 0–3 and were analyzed on day 4.

(H) Lung ILC2 and eosinophil numbers.

(I) H&E histology and severity scores. Scale bars, 100 μm.

(J) ILC2 cytokine production.

(K) IL-5 and IL-13 proteins in BALF.

(L) CGRPβ protein in BALF. Data are pooled from two independent experiments (n = 9–10 mice/group).

Mean ± SEM; unpaired t test with Welch's correction. *$p < 0.05$, **$p < 0.01$, ***$p < 0.001$, ****$p < 0.0001$, not significant (n.s.).

See also Figure S4.

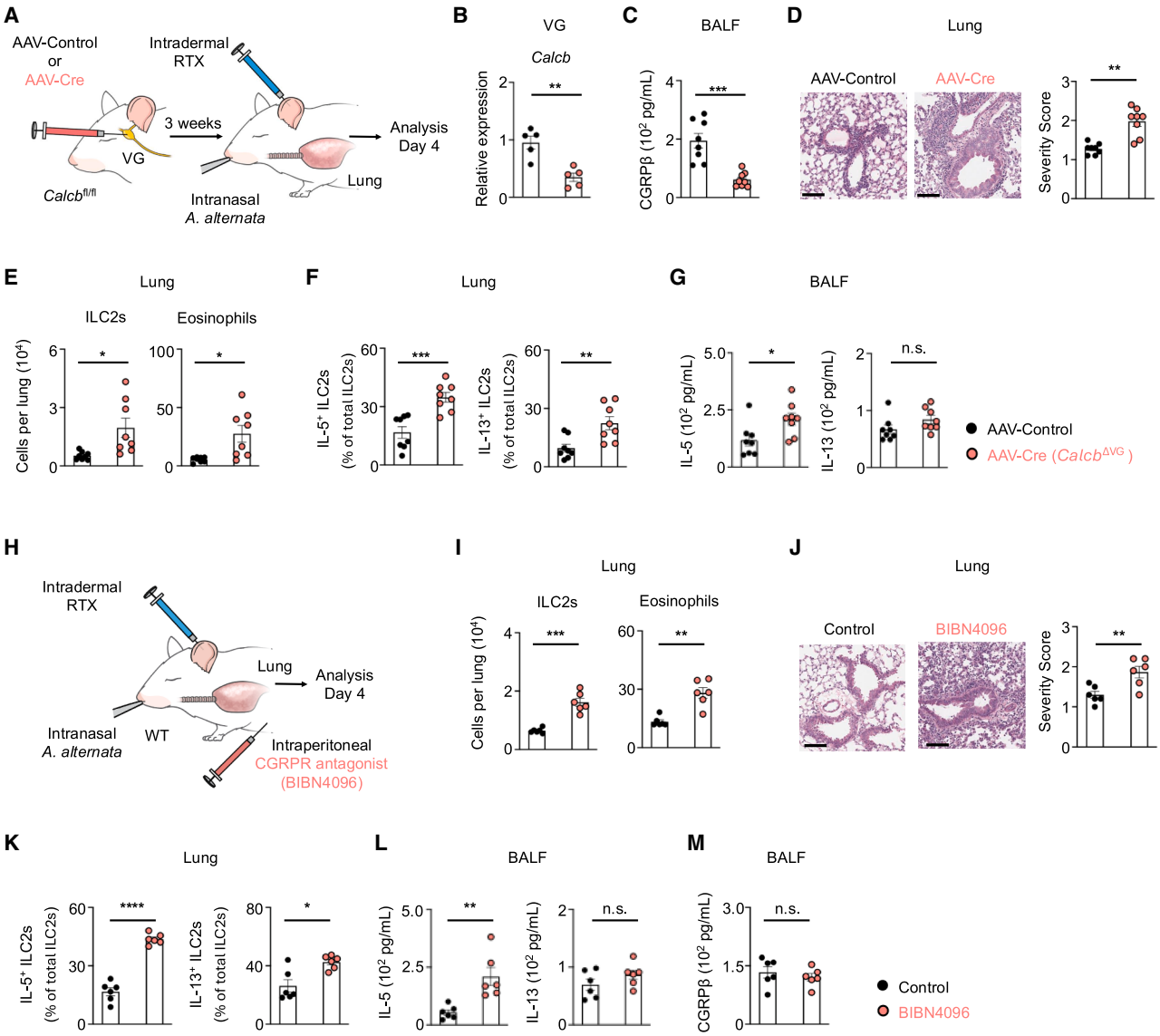


Figure 3. Deletion of *Calcb* in vagal sensory neurons disrupts the skin-lung neuroimmune circuit

(A) *Calcb*$^{fl/fl}$ mice received an intraganglionic injection of AAV9-Cre or AAV9-mCherry (AAV-Control) into the VG. 3 weeks later, mice received i.d. RTX on day 0 and intranasal *A. alternata* on days 0–3 and were analyzed on day 4.

(B) *Calcb* mRNA expression in VG.

(C) CGRPβ protein in BALF.

(D) H&E histology and severity scores. Scale bars, 100 μm.

(E) Lung ILC2 and eosinophil numbers.

(F) ILC2 cytokine production.

(G) IL-5 and IL-13 proteins in BALF. Data are pooled from two independent experiments (n = 5–8 mice/group).

(H) WT mice received i.d. RTX or vehicle on day 0 and once-daily intraperitoneal (i.p.) BIBN4096 (1 mg/kg) or vehicle on days 0–3 with intranasal *A. alternata* and were analyzed on day 4.

(I) Lung ILC2 and eosinophil numbers.

(J) H&E histology and severity scores. Scale bars, 100 μm.

(K) ILC2 cytokine production.

(L) IL-5 and IL-13 proteins in BALF.

(M) CGRPβ protein in BALF. Data are representative of two independent experiments (n = 6 mice/group).

Mean ± SEM; unpaired t test with Welch's correction. $^{*}p < 0.05$, $^{**}p < 0.01$, $^{***}p < 0.001$, $^{****}p < 0.0001$, not significant (n.s.).

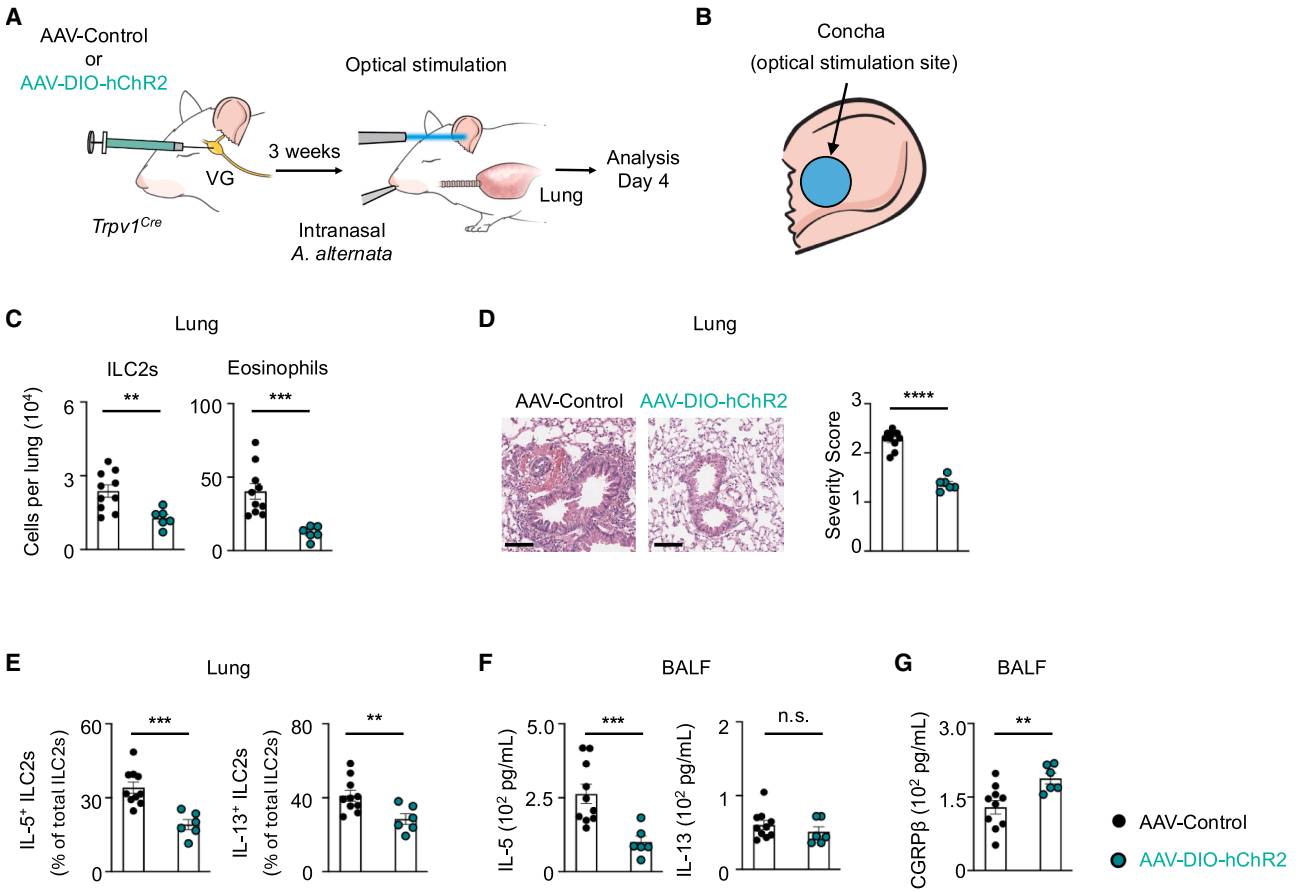


Figure 4. Optogenetic stimulation of the auricular branch of the vagus nerve in the skin suppresses allergic airway inflammation

(A) *Trpv1*^{Cre} mice received an intraganglionic injection of AAV9-DIO-hChR2 or AAV9-DIO-mCherry (AAV-Control) into the VG. 3 weeks later, mice received optical stimulation together with intranasal *A. alternata* on days 0–3 and were analyzed on day 4.

(B) Schematic of localized optogenetic stimulation applied to the conchal region of the auricle.

(C) Lung ILC2 and eosinophil numbers.

(D) H&E histology and severity scores. Scale bars, 100 μm.

(E) ILC2 cytokine production.

(F) IL-5 and IL-13 proteins in BALF.

(G) CGRPβ protein in BALF. Data are pooled from two independent experiments (n = 6–10 mice/group).

Mean ± SEM; unpaired t test with Welch's correction. $^{**}p < 0.01$, $^{***}p < 0.001$, $^{****}p < 0.0001$, not significant (n.s.).

payload of ChR2 to TRPV1^{+} vagal neurons using AAV9 in *Trpv1*^{Cre} mice (VG-*Trpv1*^{ChR2}). Following intraganglionic injection, mice received blue light illumination to the auricular skin in the setting of *A. alternata* exposure (Figures 4A and 4B). All parameters of lung inflammation were reduced in VG-*Trpv1*^{ChR2} mice (Figures 4C–4F) in association with elevated CGRPβ protein in BALF (Figure 4G). Collectively, these findings demonstrate that selective, spatially restricted activation of TRPV1^{+} vagal skin afferents suppresses allergic airway inflammation. Our study highlights that bioelectronic modulation of the auricular vagus nerve may represent a therapeutic modality to treat visceral inflammatory disorders such as asthma.

DISCUSSION

The vagus nerve has emerged as a master regulator of systemic inflammation.[44] Decades of research have uncovered sophisticated circuits by which the vagus nerve can mediate immune responses in visceral organs. A substantial conceptual advance was the identification of the CAP, in which vagal activity can dampen inflammatory cytokine production through a vagal-splenic circuit.[16,17] The most well-recognized circuit involves sensing of proinflammatory cytokines, such as tumor necrosis factor α (TNF-α) and IL-1β, which signal to the nucleus tract solitarius (NTS) in the brainstem.[45,46–53] This sensory reflex arc triggers a multitude of pathways to activate an efferent cholinergic response that ultimately triggers an anti-inflammatory cascade in the spleen.[17,54–56] Understanding the variety of stimuli, neural circuits, and neuroimmune mechanisms that underlie the CAP and other reflexes remains an area of investigation.[41]

In addition to the autonomic output of the CAP, vagal sensory neurons are intrinsically capable of directly regulating a myriad of immune processes.[3,8,9,54] Indeed, we found that pharmacological disruption of sympathetic and cholinergic pathways had a

minimal effect in our model. In the lung, sensory neurons play key roles in host defense and constrain immunopathology during infection.[8,9] The pseudounipolar structure of the sensory neuron gives it a unique dual capacity to release neuropeptides centrally not only toward the NTS[57,58] but also directly into the tissue.[59] Indeed, we show that CGRPβ release from vagal sensory neurons is an effector mechanism in this skin-lung neuroimmune reflex. One possibility by which the auricular branch could relay signals to the lung is through an unidentified CNS pathway and remains a possible area of inquiry. Another potential explanation is that this vagal interorgan reflex is mediated by neurons that exhibit axonal projections that simultaneously innervate both the lung and skin. We have recently shown that such polyorganic sensory neurons exist in the DRG and allow for interorgan communication.[15] However, our tracing data indicate that skin- and lung-innervating VG neurons are distinct populations residing in the jugular and vagal ganglia, respectively.[25,60] Thus, we speculate that the most likely possibility is that auricular sensory neurons communicate to lung-innervating sensory neurons in a relay fashion. Similar communication across sensory neurons has been reported in the TG; this axon-to-axon communication occurs via CGRP derived from unmyelinated C fibers through the nodes of Ranvier on myelinated Aδ fibers.[61] Given that both C fibers and Aδ fibers can express TRPV1, it remains unclear if, and which, fibers are communicating in our model. Future studies will be required to definitively prove such mechanisms.

Although we have identified a neuroimmune reflex mediated by the exteroceptive branch of the vagus nerve, the range of tissues and physiologic processes that are regulated by this auricular branch remains to be fully determined. Given that it innervates a region of the body that is comparatively exposed to the environment compared with other organs, it may be that this branch serves as a rheostat to coordinate internal processes in response to environmental cues such as temperature and humidity. Further, its proximity to the inner ear could regulate the sensing of elevation or pressure. Whether the auricular branch can be appropriated to promote visceral immune homeostasis across other organs, such as the intestine, remains to be clearly defined.

Impaired vagal tone has been associated with the development of autoimmunity.[62,63] Thus, in addition to direct implantation of VNS devices in conditions like RA, transcutaneous VNS is an exciting therapeutic possibility.[44,64,65] Further, understanding which specific nerve fibers mediate particular outcomes may enhance the capability of bioelectronic medicine to impact many visceral disorders. Collectively, our study highlights our expanding understanding of the vagus nerve, its role in tissue homeostasis, and its evolutionarily conserved properties that can be leveraged for future therapeutic strategies.

Limitations of the study

The precise mechanism by which vagal sensory afferents from the auricular skin (jugular ganglia) relay signals to the lung (nodose ganglia) remains unclear. Whether this is a direct axon-to-axon (e.g., interganglionic) communication and/or commences through the CNS remains to be fully defined. Additionally, it is possible that somatosensory TRPV1$^+$ neurons also contribute to such homeostatic processes. Although ATF3 labeling suggested activation of auricular vagal neurons, the precise identity of these neurons remains incompletely defined. Lastly, future studies will have to be aimed at understanding the full range of vagal nerve activation across visceral organs via the auricular branch.

RESOURCE AVAILABILITY

Lead contact

Requests for further information, resources, and reagents should be directed to and will be fulfilled by the lead contact, Brian S. Kim (bkim26@northwell.edu).

Materials availability

This study did not generate any new, unique reagents.

Data and code availability

- The data reported in this paper will be shared by the lead contact upon request.
- No original codes were generated in this study.
- Any additional information required to reanalyze the data reported in this paper is available from the lead contact upon request.

ACKNOWLEDGMENTS

This work was supported by the Allen Discovery Center program, a Paul G. Allen Frontiers Group-advised program of Allen Family Philanthropies; the National Institute of Arthritis and Musculoskeletal and Skin Diseases (AR070116, AR077007, AR080392, and P30AR079200 [R.S. and N.A.]); the National Institute of Allergy and Infectious Disease (AI167933, AI167047, and AI176660 [S.J.V.D.]); and the National Institute of Diabetes and Digestive and Kidney Diseases (NIDDK) (DK141106 to B.S.K. and H.H.; DK103901 and DK134773 to H.H.) of the National Institutes of Health. R.S. is supported by the Overseas Fellowship Grant from the Japanese Dermatological Association. N.A. is supported by the Japan Society for the Promotion of Science Program for Postdoctoral Fellowships for Research Abroad (202560622). K.S. is supported by an institutional training grant (T32 AR082315).

AUTHOR CONTRIBUTIONS

R.S. and B.S.K. conceived and designed the study. R.S., N.A., Y.A., A.B.-S., and M.T. performed the experiments and analyzed the data. R.S., K.S., N.D.R., and B.S.K. wrote the manuscript with input from all of the authors. J.K.G. created the schematics/diagrams. All of the authors provided input and reviewed the manuscript.

DECLARATION OF INTERESTS

B.S.K. is a cofounder of Alys Pharmaceuticals (Chair of the Scientific Advisory Board), Attu Therapeutics, and Neuroimmune Therapeutics. He has served as a consultant for AbbVie, Advarra (Data Safety Monitoring Committee member), Almirall, Anvia Therapeutics, Atlas Venture, Bain Capital, Cara Therapeutics, Catalys Pacific, Clexio Biosciences, Elanco, Eli Lilly, Escient Pharmaceuticals, Evommune, Galderma, General Atlantic, Gilead Sciences, Guidepoint Global, Goldman Sachs Life Sciences, Korea US Collaborative Research Fund (reviewer), Kerna Ventures, LEO Pharma (steering committee member), Medicxi, Mirador Therapeutics, Monte Rosa Therapeutics, Neurocrine Biosciences, Novartis, Orbimed, Pfizer, Propel Bio, Quilt Bio, Recludix Pharma, Regeneron, ResearchHub Foundation, Rapt Therapeutics, Resvita Bio, Sanofi, Septerna, Schrödinger, Triveni Bio, and Vida Ventures. He serves on scientific advisory boards for Attovia Therapeutics, Neurocrine Biosciences, Topo Therapeutics, Triveni Bio, and *Cell Reports Medicine* and is on the editorial board of the *Journal of Allergy and Clinical Immunology*. He is a stockholder in ABRAX Japan, Alys Pharmaceuticals, Locus Biosciences, Recens Medical, and Triveni Bio. He has received research grants from Eli Lilly and Triveni Bio.

STAR★METHODS

Detailed methods are provided in the online version of this paper and include the following:

- KEY RESOURCES TABLE
- EXPERIMENTAL MODEL AND STUDY PARTICIPANT DETAILS
  - Mice
- METHOD DETAILS
  - Allergic airway inflammation model
  - Lung histology scoring
  - Intraganglionic VG injection
  - Auricular RTX treatment
  - Chemogenetic manipulation of TRPV1$^+$ neurons
  - VG-specific deletion of Calcb
  - Optogenetic activation of TRPV1$^+$ neurons
  - CGRP receptor antagonist treatment
  - Adrenergic fiber denervation
  - Muscarinic receptor blockade
  - Nicotinic receptor blockade
  - Tracing of VG, DRG and auricular skin
  - Tissue clearing and whole-mount staining
  - Immunohistochemistry
  - VG neuronal culture and Ca^{2+} imaging
  - Flow cytometry
  - ELISA
  - Real-time qPCR
- QUANTIFICATION AND STATISTICAL ANALYSIS

SUPPLEMENTAL INFORMATION

Supplemental information can be found online at https://doi.org/10.1016/j.immuni.2026.06.005.

Received: January 8, 2026
Revised: April 8, 2026
Accepted: June 10, 2026
Published: July 15, 2026

REFERENCES

1. Steinman, L. (2004). Elaborate interactions between the immune and nervous systems. Nat. Immunol. *5*, 575–581. https://doi.org/10.1038/ni1078.
2. Perner, C., Flayer, C.H., Zhu, X., Aderhold, P.A., Dewan, Z.N.A., Voisin, T., Camire, R.B., Chow, O.A., Chiu, I.M., and Sokol, C.L. (2020). Substance P Release by Sensory Neurons Triggers Dendritic Cell Migration and Initiates the Type-2 Immune Response to Allergens. Immunity *53*, 1063–1077.e7. https://doi.org/10.1016/j.immuni.2020.10.001.
3. Tamari, M., Del Bel, K.L., Ver Heul, A.M., Zamidar, L., Orimo, K., Hoshi, M., Trier, A.M., Yano, H., Yang, T.L., Biggs, C.M., et al. (2024). Sensory neurons promote immune homeostasis in the lung. Cell *187*, 44–61.e17. https://doi.org/10.1016/j.cell.2023.11.027.
4. Wallrapp, A., Burkett, P.R., Riesenfeld, S.J., Kim, S.J., Christian, E., Abdulnour, R.E.E., Thakore, P.I., Schnell, A., Lambden, C., Herbst, R.H., et al. (2019). Calcitonin Gene-Related Peptide Negatively Regulates Alarmin-Driven Type 2 Innate Lymphoid Cell Responses. Immunity *51*, 709–723.e6. https://doi.org/10.1016/j.immuni.2019.09.005.
5. Lu, Y.Z., Nayer, B., Singh, S.K., Alshoubaki, Y.K., Yuan, E., Park, A.J., Maruyama, K., Akira, S., and Martino, M.M. (2024). CGRP sensory neurons promote tissue healing via neutrophils and macrophages. Nature *628*, 604–611. https://doi.org/10.1038/s41586-024-07237-y.
6. Riol-Blanco, L., Ordovas-Montanes, J., Perro, M., Naval, E., Thiriot, A., Alvarez, D., Paust, S., Wood, J.N., and von Andrian, U.H. (2014). Nociceptive sensory neurons drive interleukin-23-mediated psoriasiform skin inflammation. Nature *510*, 157–161. https://doi.org/10.1038/nature13199.
7. Talbot, S., Abdulnour, R.E.E., Burkett, P.R., Lee, S., Cronin, S.J.F., Pascal, M.A., Laedermann, C., Foster, S.L., Tran, J.V., Lai, N., et al. (2015). Silencing Nociceptor Neurons Reduces Allergic Airway Inflammation. Neuron *87*, 341–354. https://doi.org/10.1016/j.neuron.2015.06.007.
8. Baral, P., Umans, B.D., Li, L., Wallrapp, A., Bist, M., Kirschbaum, T., Wei, Y., Zhou, Y., Kuchroo, V.K., Burkett, P.R., et al. (2018). Nociceptor sensory neurons suppress neutrophil and γδ T cell responses in bacterial lung infections and lethal pneumonia. Nat. Med. *24*, 417–426. https://doi.org/10.1038/nm.4501.
9. Almanzar, N., Yang, D., Xia, J., Udit, S., Joshi, P., Adhikari, S., Hoagland, D.A., Yeung, S.T., Khairallah, C., Huerta, T., et al. (2025). Vagal TRPV1(+) sensory neurons protect against influenza virus infection by regulating lung myeloid cell dynamics. Sci. Immunol. *10*, eads6243. https://doi.org/10.1126/sciimmunol.ads6243.
10. Cohen, J.A., Edwards, T.N., Liu, A.W., Hirai, T., Jones, M.R., Wu, J., Li, Y., Zhang, S., Ho, J., Davis, B.M., et al. (2019). Cutaneous TRPV1+ Neurons Trigger Protective Innate Type 17 Anticipatory Immunity. Cell *178*, 919–932.e14. https://doi.org/10.1016/j.cell.2019.06.022.
11. Kashem, S.W., Riedl, M.S., Yao, C., Honda, C.N., Vulchanova, L., and Kaplan, D.H. (2015). Nociceptive Sensory Fibers Drive Interleukin-23 Production from CD301b+ Dermal Dendritic Cells and Drive Protective Cutaneous Immunity. Immunity *43*, 515–526. https://doi.org/10.1016/j.immuni.2015.08.016.
12. Lai, N.Y., Musser, M.A., Pinho-Ribeiro, F.A., Baral, P., Jacobson, A., Ma, P., Potts, D.E., Chen, Z., Paik, D., Soualhi, S., et al. (2020). Gut-Innervating Nociceptor Neurons Regulate Peyer's Patch Microfold Cells and SFB Levels to Mediate Salmonella Host Defense. Cell *180*, 33–49.e22. https://doi.org/10.1016/j.cell.2019.11.014.
13. Hoeffel, G., Debroas, G., Roger, A., Rossignol, R., Gouilly, J., Laprie, C., Chasson, L., Barbon, P.V., Balsamo, A., Reynders, A., et al. (2021). Sensory neuron-derived TAFA4 promotes macrophage tissue repair functions. Nature *594*, 94–99. https://doi.org/10.1038/s41586-021-03563-7.
14. Enamorado, M., Kulalert, W., Han, S.J., Rao, I., Delaleu, J., Link, V.M., Yong, D., Smelkinson, M., Gil, L., Nakajima, S., et al. (2023). Immunity to the microbiota promotes sensory neuron regeneration. Cell *186*, 607–620.e17. https://doi.org/10.1016/j.cell.2022.12.037.
15. Kim, B., Wang, Z., Meng, X., Xie, Z., Hor, C.C., Zhang, W., Li, X., Song, K., Auyeung, K., Iriki, H., et al. (2025). An interorgan neuroimmune circuit promotes visceral hypersensitivity. Res. Sq. rs.3.rs-6221928. https://doi.org/10.21203/rs.3.rs-6221928/v1.
16. Borovikova, L.V., Ivanova, S., Zhang, M., Yang, H., Botchkina, G.I., Watkins, L.R., Wang, H., Abumrad, N., Eaton, J.W., and Tracey, K.J. (2000). Vagus nerve stimulation attenuates the systemic inflammatory response to endotoxin. Nature *405*, 458–462. https://doi.org/10.1038/35013070.
17. Wang, H., Yu, M., Ochani, M., Amella, C.A., Tanovic, M., Susarla, S., Li, J.H., Wang, H., Yang, H., Ulloa, L., et al. (2003). Nicotinic acetylcholine receptor alpha7 subunit is an essential regulator of inflammation. Nature *421*, 384–388. https://doi.org/10.1038/nature01339.
18. Tracey, K.J. (2002). The inflammatory reflex. Nature *420*, 853–859. https://doi.org/10.1038/nature01321.
19. Tesser, J.R.P., Crowley, A.R., Box, E.J., June, J.P., Wickersham, P.B., Valenzuela, G.J., Gaylis, N.B., Lam, G.K.W., Pacheco, L.A., Ridley, D.J., et al. (2025). Vagus nerve-mediated neuroimmune modulation for rheumatoid arthritis: a pivotal randomized controlled trial. Nat. Med. *32*, 369–378. https://doi.org/10.1038/s41591-025-04114-7.
20. Peuker, E.T., and Filler, T.J. (2002). The nerve supply of the human auricle. Clin. Anat. *15*, 35–37. https://doi.org/10.1002/ca.1089.
21. Butt, M.F., Albusoda, A., Farmer, A.D., and Aziz, Q. (2020). The anatomical basis for transcutaneous auricular vagus nerve stimulation. J. Anat. *236*, 588–611. https://doi.org/10.1111/joa.13122.
22. Badran, B.W., Brown, J.C., Dowdle, L.T., Mithoefer, O.J., LaBate, N.T., Coatsworth, J., DeVries, W.H., Austelle, C.W., McTeague, L.M., Yu, A.,

et al. (2018). Tragus or cymba conchae? Investigating the anatomical foundation of transcutaneous auricular vagus nerve stimulation (taVNS). Brain Stimul. *11*, 947–948. https://doi.org/10.1016/j.brs.2018.06.003.

23. Wang, Y., Li, S.Y., Wamg, D., Wu, M.Z., He, J.K., Zhang, J.L., Zhao, B., Hou, L.W., Wang, J.Y., Wang, L., et al. (2021). Transcutaneous Auricular Vagus Nerve Stimulation: From Concept to Application. Neuroschi Bull *37*, 853–862. https://doi.org/10.1007/s12264-020-00619-y.
24. Yakunina, N., Kim, S.S., and Nam, E.C. (2017). Optimization of Transcutaneous Vagus Nerve Stimulation Using Functional MRI. Neuromodulation *20*, 290–300. https://doi.org/10.1111/ner.12541.
25. Su, Y., Barr, J., Jaquish, A., Xu, J., Verheyden, J.M., and Sun, X. (2022). Identification of lung innervating sensory neurons and their target specificity. Am J Physiol Lung Cell Mol Physiol *322*, L50–L63. https://doi.org/10.1152/ajplung.00376.2021.
26. Bartemes, K.R., Iijima, K., Kobayashi, T., Kephart, G.M., McKenzie, A.N., and Kita, H. (2012). IL-33 responsive lineage-CD25+ CD44(hi) lymphoid cells mediate innate type 2 immunity and allergic inflammation in the lungs. J Immunol *188*, 1503–1513. https://doi.org/10.4049/jimmunol.1102832.
27. Zhou, W., Toki, S., Zhang, J., Goleniewksa, K., Newcomb, D.C., Cephus, J.Y., Dulek, D.E., Bloodworth, M.H., Stier, M.T., Polosuhkin, V., et al. (2016). Prostaglandin I2 Signaling and Inhibition of Group 2 Innate Lymphoid Cell Responses. Am J Respir Crit Care Med *193*, 31–42. https://doi.org/10.1164/rccm.201410-1793OC.
28. Thio, C.L., Chi, P.Y., Lai, A.C., and Chang, Y.J. (2018). Regulation of type 2 innate lymphoid cell-dependent airway hyperreactivity by butyrate. J Allergy Clin Immunol 142, 1867-1883 e1812. 10.1016/j.jaci.2018.02.032.
29. Jeffry, J.A., Yu, S.Q., Sikand, P., Parihar, A., Evans, M.S., and Premkumar, L.S. (2009). Selective targeting of TRPV1 expressing sensory nerve terminals in the spinal cord for long lasting analgesia. PLoS One *4*, e7021. https://doi.org/10.1371/jounal.pone.0007021.
30. Szallasi, A., Szallasi, Z., and Blumberg, P.M. (1990). Permanent effects of neonatally administered resiniferatoxin in the rat. Brain Res *537*, 182–186. https://doi.org/10.1016/0006-8993(90)90356-g.
31. Raisinghani, M., Pabbidi, R.M., and Premkumar, L.S. (2005). Activation of transient receptor potential vanilloid 1 (TRPV1) by resiniferatoxin. J Physiol *567*, 771–786. https://doi.org/10.1113/jphysiol.2005.087874.
32. Flayer, C.H., Kernin, I.J., Matatia, P.R., Zeng, X., Yarmolinsky, D.A., Han, C., Naik, P.R., Buttaci, D.R., Aderhold, P.A., Camire, R.B., et al. (2024). A gammadelta T cell-IL-3 axis controls allergic responses through sensory neurons. Nature *634*, 440–446. https://doi.org/10.1038/s41586-024-07869-0.
33. Tsujino, H., Kondo, E., Fukuoka, T., Dai, Y., Tokunaga, A., Miki, K., Yonenobu, K., Ochi, T., and Noguchi, K. (2000). Activating transcription factor 3 (ATF3) induction by axotomy in sensory and motoneurons: A novel neuronal marker of nerve injury. Mol. Cell. Neurosci. *15*, 170–182. https://doi.org/10.1006/mcne.1999.0814.
34. Bráz, J.M., and Basbaum, A.I. (2010). Differential ATF3 expression in dorsal root ganglion neurons reveals the profile of primary afferents engaged by diverse noxious chemical stimuli. Pain *150*, 290–301. https://doi.org/10.1016/j.pain.2010.05.005.
35. Delaleu, J., Burstein, V., Ansaldo, E., Becaccece, I., Nagai, M., Bouladoux, N., Corral, D., Muñoz Zamora, A., Ayash, A., Smelkinson, M., et al. (2025). Maladaptive immunity to the microbiota promotes neuronal hyperinnervation and itch via IL-17A. Proc. Natl. Acad. Sci. USA *122*, e2525146122. https://doi.org/10.1073/pnas.2525146122.
36. Kaelberer, M.M., Caceres, A.I., and Jordt, S.E. (2020). Activation of a nerve injury transcriptional signature in airway-innervating sensory neurons after lipopolysaccharide-induced lung inflammation. Am. J. Physiol., Lung Cell. Mol. Physiol. *318*, L953–L964. https://doi.org/10.1152/ajplung.00403.2019.
37. Armbruster, B.N., Li, X., Pausch, M.H., Herlitze, S., and Roth, B.L. (2007). Evolving the lock to fit the key to create a family of G protein-coupled receptors potently activated by an inert ligand. Proc Natl Acad Sci U S A *104*, 5163–5168. https://doi.org/10.1073/pnas.0700293104.
38. Alexander, G.M., Rogan, S.C., Abbas, A.I., Armbruster, B.N., Pei, Y., Allen, J.A., Nonneman, R.J., Hartmann, J., Moy, S.S., Nicolelis, M.A., et al. (2009). Remote control of neural activity in transgenic mice expressing evolved G protein-coupled receptors. Neuron *63*, 27–39. https://doi.org/10.1016/j.neuron.2009.06.014.
39. DeRose, V., Robbins, R.A., Snider, R.M., Spurzem, J.R., Thiele, G.M., Rennard, S.I., and Rubinstein, I. (1994). Substance P increases neutrophil adhesion to bronchial epithelial cells. J. Immunol. *152*, 1339–1346. https://doi.org/10.4049/jimmunol.152.3.1339.
40. Lv, X., Chen, Q., Zhang, Z., Du, K., Huang, Y., Li, X., and Zeng, Y. (2023). αCGRP deficiency aggravates pulmonary fibrosis by activating the PPARγ signaling pathway. Genes Immun. *24*, 139–148. https://doi.org/10.1038/s41435-023-00206-x.
41. Hiroki, C.H., Hassanabad, M.F., Defaye, M., Sarden, N., Bartlett, A., Farias, R., Nguyen, A.P., Guerrero-Fonseca, I.M., Yoon, G., Brown, L., et al. (2025). Nociceptor neurons suppress alveolar macrophage-induced Siglec-F+ neutrophil-mediated inflammation to protect against pulmonary fibrosis. Immunity *58*, 2054–2068.e6. https://doi.org/10.1016/j.immuni.2025.05.002.
42. Nagel, G., Szellas, T., Huhn, W., Kateriya, S., Adeishvili, N., Berthold, P., Ollig, D., Hegemann, P., and Bamberg, E. (2003). Channelrhodopsin-2, a directly light-gated cation-selective membrane channel. Proc. Natl. Acad. Sci. USA *100*, 13940–13945. https://doi.org/10.1073/pnas.1936192100.
43. Boyden, E.S., Zhang, F., Bamberg, E., Nagel, G., and Deisseroth, K. (2005). Millisecond-timescale, genetically targeted optical control of neural activity. Nat. Neurosci. *8*, 1263–1268. https://doi.org/10.1038/nn1525.
44. Sahn, B., Pascuma, K., Kohn, N., Tracey, K.J., and Markowitz, J.F. (2023). Transcutaneous auricular vagus nerve stimulation attenuates inflammatory bowel disease in children: a proof-of-concept clinical trial. Bioelectron. Med. *9*, 23. https://doi.org/10.1186/s42234-023-00124-3.
45. Goehler, L.E., Gaykema, R.P., Hammack, S.E., Maier, S.F., and Watkins, L.R. (1998). Interleukin-1 induces c-Fos immunoreactivity in primary afferent neurons of the vagus nerve. Brain Res. *804*, 306–310. https://doi.org/10.1016/s0006-8993(98)00685-4.
46. Zanos, T.P., Silverman, H.A., Levy, T., Tsaava, T., Battinelli, E., Lorraine, P.W., Ashe, J.M., Chavan, S.S., Tracey, K.J., and Bouton, C.E. (2018). Identification of cytokine-specific sensory neural signals by decoding murine vagus nerve activity. Proc. Natl. Acad. Sci. USA *115*, E4843–E4852. https://doi.org/10.1073/pnas.1719083115.
47. Silverman, H.A., Tynan, A., Hepler, T.D., Chang, E.H., Gunasekaran, M., Li, J.H., Huerta, T.S., Tsaava, T., Chang, Q., Addorisio, M.E., et al. (2023). Transient Receptor Potential Ankyrin-1-expressing vagus nerve fibers mediate IL-1beta induced hypothermia and reflex anti-inflammatory responses. Mol. Med. *29*, 4. https://doi.org/10.1186/s10020-022-00590-6.
48. Ek, M., Kurosawa, M., Lundeberg, T., and Ericsson, A. (1998). Activation of vagal afferents after intravenous injection of interleukin-1beta: role of endogenous prostaglandins. J. Neurosci. *18*, 9471–9479. https://doi.org/10.1523/JNEUROSCI.18-22-09471.1998.
49. Hosoi, T., Okuma, Y., and Nomura, Y. (2000). Electrical stimulation of afferent vagus nerve induces IL-1beta expression in the brain and activates HPA axis. Am. J. Physiol. Regul. Integr. Comp. Physiol. *279*, R141–R147. https://doi.org/10.1152/ajpregu.2000.279.1.R141.
50. Emch, G.S., Hermann, G.E., and Rogers, R.C. (2001). TNF-alpha-induced c-Fos generation in the nucleus of the solitary tract is blocked by NBQX and MK-801. Am. J. Physiol. Regul. Integr. Comp. Physiol. *281*, R1394–R1400. https://doi.org/10.1152/ajpregu.2001.281.5.R1394.
51. Steinberg, B.E., Silverman, H.A., Robbiati, S., Gunasekaran, M.K., Tsaava, T., Battinelli, E., Stiegler, A., Bouton, C.E., Chavan, S.S., Tracey, K.J., et al. (2016). Cytokine-specific Neurograms in the Sensory Vagus Nerve. Bioelectron. Med. *3*, 7–17. https://doi.org/10.15424/bioelectronmed.2016.00007.
52. Jin, H., Li, M., Jeong, E., Castro-Martinez, F., and Zuker, C.S. (2024). A body-brain circuit that regulates body inflammatory responses. Nature *630*, 695–703. https://doi.org/10.1038/s41586-024-07469-y.
53. Prescott, S.L., Umans, B.D., Williams, E.K., Brust, R.D., and Liberles, S.D. (2020). An Airway Protection Program Revealed by Sweeping Genetic

Control of Vagal Afferents. Cell *181*, 574–589.e14. https://doi.org/10.1016/j.cell.2020.03.004.

54. Rosas-Ballina, M., Ochani, M., Parrish, W.R., Ochani, K., Harris, Y.T., Huston, J.M., Chavan, S., and Tracey, K.J. (2008). Splenic nerve is required for cholinergic antiinflammatory pathway control of TNF in endotoxemia. Proc. Natl. Acad. Sci. USA *105*, 11008–11013. https://doi.org/10.1073/pnas.0803237105.
55. Rosas-Ballina, M., Olofsson, P.S., Ochani, M., Valdés-Ferrer, S.I., Levine, Y.A., Reardon, C., Tusche, M.W., Pavlov, V.A., Andersson, U., Chavan, S., et al. (2011). Acetylcholine-synthesizing T cells relay neural signals in a vagus nerve circuit. Science *334*, 98–101. https://doi.org/10.1126/science.1209985.
56. Andersson, U., and Tracey, K.J. (2012). Neural reflexes in inflammation and immunity. J. Exp. Med. *209*, 1057–1068. https://doi.org/10.1084/jem.20120571.
57. Prescott, S.L., and Liberles, S.D. (2022). Internal senses of the vagus nerve. Neuron *110*, 579–599. https://doi.org/10.1016/j.neuron.2021.12.020.
58. Andresen, M.C., Fawley, J.A., and Hofmann, M.E. (2012). Peptide and lipid modulation of glutamatergic afferent synaptic transmission in the solitary tract nucleus. Front Neurosci *6*, 191. https://doi.org/10.3389/fnins.2012.00191.
59. Iyengar, S., Ossipov, M.H., and Johnson, K.W. (2017). The role of calcitonin gene-related peptide in peripheral and central pain mechanisms including migraine. Pain *158*, 543–559. https://doi.org/10.1097/j.pain.0000000000000831.
60. Neuhuber, W.L., and Berthoud, H.R. (2021). Functional anatomy of the vagus system - Emphasis on the somato-visceral interface. Auton Neurosci *236*, 102887. https://doi.org/10.1016/j.autneu.2021.102887.
61. Edvinsson, J.C.A., Warfvinge, K., Krause, D.N., Blixt, F.W., Sheykhzade, M., Edvinsson, L., and Haanes, K.A. (2019). C-fibers may modulate adjacent Adelta-fibers through axon-axon CGRP signaling at nodes of Ranvier in the trigeminal system. J Headache Pain *20*, 105. https://doi.org/10.1186/s10194-019-1055-3.
62. Williams, D.P., Koenig, J., Carnevali, L., Sgoifo, A., Jarczok, M.N., Sternberg, E.M., and Thayer, J.F. (2019). Heart rate variability and inflammation: A meta-analysis of human studies. Brain Behav. Immun. *80*, 219–226. https://doi.org/10.1016/j.bbi.2019.03.009.
63. Koopman, F.A., Tang, M.W., Vermeij, J., de Hair, M.J., Choi, I.Y., Vervoordeldonk, M.J., Gerlag, D.M., Karemaker, J.M., and Tak, P.P. (2016). Autonomic Dysfunction Precedes Development of Rheumatoid Arthritis: A Prospective Cohort Study. EBiomedicine *6*, 231–237. https://doi.org/10.1016/j.ebiom.2016.02.029.
64. Baker, M.C., Kavanagh, S., Cohen, S., Matsumoto, A.K., Dikranian, A., Tesser, J., Kivitz, A., Alataris, K., and Genovese, M.C. (2023). A Randomized, Double-Blind, Sham-Controlled, Clinical Trial of Auricular Vagus Nerve Stimulation for the Treatment of Active Rheumatoid Arthritis. Arthritis Rheumatol. *75*, 2107–2115. https://doi.org/10.1002/art.42637.
65. Steyn, E., Mohamed, Z., and Husselman, C. (2013). Non-invasive vagus nerve stimulation for the treatment of acute asthma exacerbations-results from an initial case series. Int. J. Emerg. Med. *6*, 7. https://doi.org/10.1186/1865-1380-6-7.
66. Braber, S., Henricks, P.A.J., Nijkamp, F.P., Kraneveld, A.D., and Folkerts, G. (2010). Inflammatory changes in the airways of mice caused by cigarette smoke exposure are only partially reversed after smoking cessation. Respir. Res. *11*, 99. https://doi.org/10.1186/1465-9921-11-99.
67. Han, W., and de Araujo, I.E. (2021). Dissection and surgical approaches to the mouse jugular-nodose ganglia. STAR Protoc. *2*, 100474. https://doi.org/10.1016/j.xpro.2021.100474.

CellPress
OPEN ACCESS

STAR★METHODS

KEY RESOURCES TABLE

REAGENT or RESOURCE	SOURCE	IDENTIFIER
Antibodies		
Rabbit anti-CGRP antibody	BMA Biomedicals	Cat# T-4032; RRID: AB_518147
Rabbit anti-ATF3 antibody	Novus Biologicals	Cat# NBP1-85816; RRID: AB_11014863
Donkey anti-rabbit Alexa Fluor 594 secondary antibody	Thermo Fisher Scientific	Cat# A-21207; RRID: AB_141637
Anti-CD16/32 antibody	Bio X Cell	Cat# BE0307
Zombie NIR viability dye	BioLegend	Cat# 423105; RRID: AB_2876352
Anti-mouse CD3 antibody	BioLegend	Cat# 100268; RRID: AB_2876392
Anti-mouse CD4 antibody	BioLegend	Cat# 100449; RRID: AB_2564587
Anti-mouse CD8b antibody	Thermo Fisher Scientific (eBioscience)	Cat# 62-0083-82; RRID: AB_2744768
Anti-mouse/human CD11b antibody	BioLegend	Cat# 101233; RRID: AB_10896949
Anti-mouse CD11c antibody	Thermo Fisher Scientific (eBioscience)	Cat# 45-0114-82; RRID: AB_925727
Anti-mouse CD45 antibody	Invitrogen	Cat# 58-0451-82; RRID: AB_11218871
Anti-mouse CD45R/B220 antibody	BioLegend	Cat# 103275; RRID: AB_2860602
Anti-mouse CD90.2 antibody	BD Biosciences	Cat# 740442; RRID: AB_2740169
Anti-mouse CD117 (c-Kit) antibody	BioLegend	Cat# 105838; RRID: AB_2616739
Anti-mouse CD127 (IL-7Ra) antibody	BioLegend	Cat# 135013; RRID: AB_1937266
Anti-mouse CD127 (IL-7Ra) antibody	BioLegend	Cat# 135035; RRID: AB_2564577
Anti-mouse Siglec-F antibody	BD Biosciences	Cat# 562757; RRID: AB_2687994
Anti-mouse/human KLRG1 (MAFA) antibody	BioLegend	Cat# 138419; RRID: AB_2563357
Anti-mouse Ly6A/E (Sca-1) antibody	BD Biosciences	Cat# 749199; RRID: AB_2873577
Anti-mouse Ly-6G antibody	BioLegend	Cat# 127666; RRID: AB_2876454
Anti-mouse IL-5 antibody	BioLegend	Cat# 504306; RRID: AB_315330
Anti-mouse IL-13 antibody	Thermo Fisher Scientific (eBioscience)	Cat# 25-7133-82; RRID: AB_2573530
Bacterial and virus strains		
AAV9-hSyn-DIO-hM3Dq(Gq)-mCherry	Addgene	Cat# 44361-AAV9
AAV9-hSyn-DIO-mCherry	Addgene	Cat# 50459-AAV9
AAV9-hSyn-DIO-hM4Di(Gi)-mCherry	Addgene	Cat# 44362-AAV9
pENN-AAV9-hSyn-Cre-hGH	Addgene	Cat# 105555-AAV9
AAV9-hSyn-mCherry	Addgene	Cat# 114472-AAV9
AAV9-hSyn-DIO-hChR2(H134R)-EGFP-WPRE-hGH polyA	BrainVTA	Cat# PT-4358
AAV2-retro-Cre	VectorBuilder	Cat# VB220605-1075ztp
Chemicals, peptides, and recombinant proteins		
Alternaria alternata extract	Greer Laboratories	Cat# NC1620293
Resiniferatoxin (RTX)	Alomone Labs	Cat# R-400
Clozapine-N-oxide (CNO)	Tocris	Cat# 6329
BIBN4096	MedChemExpress	Cat# HY-10095
6-Hydroxydopamine (6-OHDA)	Sigma-Aldrich	Cat# H4381
Ascorbic acid	Sigma-Aldrich	Cat# PHR1008
Glycopyrrolate	Sigma-Aldrich	Cat# SML0029
Mecamylamine hydrochloride	Sigma-Aldrich	Cat# M9020
WGA-Alexa Fluor 647	Thermo Fisher Scientific	Cat# W32466
WGA-Alexa Fluor 488	Thermo Fisher Scientific	Cat# W11261

(*Continued on next page*)

Continued		
REAGENT or RESOURCE	SOURCE	IDENTIFIER
CTB-Alexa Fluor 488	Thermo Fisher Scientific	Cat# C34775
CTB-Alexa Fluor 647	Thermo Fisher Scientific	Cat# C34778
Papain	Worthington Biochemical	Cat# LS003124
Collagenase type I	Worthington Biochemical	Cat# LS004196
Dispase	Gibco	Cat# 17105041
Mouse NGF 2.5S Native Protein	Gibco	Cat# 13257-019
Phorbol 12-myristate 13-acetate	Sigma-Aldrich	Cat# P1585
Ionomycin	Invitrogen	Cat# I24222
Brefeldin A	BioLegend	Cat# 420601
Monensin	BioLegend	Cat# 420701
Critical commercial assays		
Mouse IL-5 DuoSet ELISA Kit	R&D Systems	Cat# DY405
Mouse IL-13 DuoSet ELISA Kit	R&D Systems	Cat# DY413
Substance P ELISA kit	Enzo Life Sciences	Cat# ADI-900-018A
Mouse CGRP1 ELISA Kit	MyBioSource	Cat# MBS2509891
Mouse CGRP2 ELISA Kit	MyBioSource	Cat# MBS7241942
RNeasy Plus Micro Kit	QIAGEN	Cat# 74034
QuantiTect Reverse Transcription Kit	QIAGEN	Cat# 205311
TaqMan Fast Advanced Master Mix	Thermo Fisher Scientific	Cat# 4444556
Experimental models: Organisms/strains		
Mouse: C57BL/6J	The Jackson Laboratory	JAX: 000664
Mouse: *Rosa26*$^{LSL\text{-}tdTomato}$	The Jackson Laboratory	JAX: 007909
Mouse: *Trpv1*^{Cre}	The Jackson Laboratory	JAX: 017769
Mouse: *Rosa26*$^{LSL\text{-}hM3Dq}$	The Jackson Laboratory	JAX: 026942
Mouse: *Rosa26*$^{LSL\text{-}hM4Di}$	The Jackson Laboratory	JAX: 026219
Mouse: Pirt-GCaMP3	Hongzhen Hu	N/A
Mouse: *Calcb*$^{fl/fl}$	Hongzhen Hu	N/A
Mouse: *Trpv1*^{hM3Dq}	This paper	N/A
Mouse: *Trpv1*^{hM4Di}	This paper	N/A
Oligonucleotides		
TaqMan assay: *Calcb*	Thermo Fisher Scientific	Cat# Mm00446495_m1
TaqMan assay: *Gapdh*	Thermo Fisher Scientific	Cat# Mm99999915_g1
Software and algorithms		
Zen Blue	Zeiss	N/A
Fiji/ImageJ	NIH; Fiji	https://fiji.sc/; https://imagej.nih.gov/ij/
GraphPad Prism 9.0	GraphPad Software	https://www.graphpad.com/
FlowJo 10	Tree Star	https://www.flowjo.com/
Other		
Leica Stellaris8 confocal microscope	Leica Microsystems	N/A
Cytek Aurora flow cytometer	Cytek Biosciences	N/A
Zeiss Axio Observer 8 microscope	Zeiss	N/A
gentleMACS Dissociator with Heaters	Miltenyi Biotec	N/A
Applied Biosystems QuantStudio 6 Pro	Thermo Fisher Scientific	N/A

EXPERIMENTAL MODEL AND STUDY PARTICIPANT DETAILS

Mice

C57BL/6J wild-type (WT; JAX 000664), R26-LSL-tdTomato (Ai9; JAX 007909), *Trpv1*^{Cre} (JAX 017769), R26-LSL-Gq-DREADD (JAX 026942), and R26-LSL-Gi-DREADD (JAX 026219) mice were purchased from the Jackson Laboratory. Pirt-GCaMP3 and *Calcb*$^{fl/fl}$ mice were provided by Dr. Hongzhen Hu (Icahn School of Medicine at Mount Sinai, New York, USA). TRPV1-hM3Dq mice were

generated by crossing *Trpv1*^{Cre} mice with R26-LSL-Gq-DREADD mice. TRPV1-hM4Di mice were generated by crossing *Trpv1*^{Cre} mice with R26-LSL-Gi-DREADD mice. All mice were housed in specific-pathogen-free (SPF) conditions and environmentally controlled animal facilities with a 12-hr light-dark cycle and were given unrestricted access to food and water. Mice 7–12 weeks of age were used. Sex is indicated below. *Wild-type* and *Calcb*$^{fl/fl}$ experiments were performed using female mice. In *Trpv1*^{Cre}-based experiments, both male and female mice were used to increase cohort size, as sufficient numbers of age-matched animals were not always available within a single cohort. Otherwise, animals were assigned to experimental groups in an age-matched manner, and littermates were used whenever possible. All animal protocols and experiments were approved by the Institutional Animal Care and Use Committee (IACUC) of the Icahn School of Medicine at Mount Sinai and performed in accordance with the guidelines of the National Institutes of Health, USA.

METHOD DETAILS

Allergic airway inflammation model

Mice were lightly anesthetized with 3.5% isoflurane and intranasally administered *A. alternata* extract (Greer Laboratories, NC1620293, 2 μg/40 μL of sterile phosphate-buffered saline (PBS)) for four consecutive days (days 0–3). Mice were sacrificed on day 4, approximately 15 hrs after the final intranasal *A. alternata* challenge, for histological and immunologic analysis. Lungs were collected following PBS perfusion and were processed for immune cell analysis by flow cytometry (right lungs) or fixed in 4% paraformaldehyde for histological analysis (left lungs). Histology slides and digital images were created by HistoWiz (histowiz.com).

Lung histology scoring

Lung inflammation was scored as previously described.[66] The degree of peribronchial and perivascular inflammation was evaluated on a semiquantitative scale of 0–3. A score of 0 was assigned when no inflammation was detectable; a score of 1 when occasional cuffing with inflammatory cells was observed; a score of 2 when most bronchi or vessels were surrounded by a thin layer of inflammatory cells (one to five cells thick); and a score of 3 when most bronchi or vessels were surrounded by a thick layer of inflammatory cells (more than five cells thick). For each mouse, one representative lung section was selected, and five predefined airway/vessel regions within the lung parenchyma were evaluated on that section. Total lung inflammation was defined as the average of the peribronchial and perivascular inflammation scores. Lung histology was scored by an investigator blinded to treatment group.

Intraganglionic VG injection

Intraganglionic injection into the vagal ganglia (VG) was performed as previously described.[67] In brief, mice were anesthetized with 2% isoflurane and placed supine on a heated stage. After aseptic preparation of the ventral neck, a midline cervical incision was made, and the infrahyoid muscles were bluntly separated to expose the carotid sheath. The VG was identified rostral to the carotid bifurcation under an operating microscope. A NanoFil microsyringe (WPI) connected to a remote infusion pump (Harvard Apparatus) was loaded with WGA-Alexa Fluor 647 (WGA-AF647) or AAV9 vectors depending on the experiments. The 36G beveled NanoFil needle was advanced into the VG, and the virus was delivered bilaterally in a volume of 0.5 μL per side at a rate of 2 nL/s. The needle was left in place for 2 min to minimize reflux before a slow withdrawal. Animals recovered on a heated pad and were monitored daily for weight, grooming, posture, and incision integrity. Experiments were performed 3 weeks after injection to allow for transgene expression. Injection accuracy was assessed in a subset of animals based on the expected reporter expression pattern in the VG, together with auricular skin labeling. Formal blinded assessment of injection site verification was not performed.

Auricular RTX treatment

To selectively activate TRPV1$^+$ channels in the auricular skin, RTX (Alomone Labs, R-400, 100 ng/ear) was prepared in saline and administered i.d. to the central dorsal aspect of the auricle 1 hr before intranasal *A. alternata* challenge on day 0. Mice were lightly anesthetized with 3.5% isoflurane during the procedure. Control mice received saline.

Chemogenetic manipulation of TRPV1$^+$ neurons

Unless otherwise indicated, chemogenetic manipulation was induced by an i.d. injection of clozapine-N-oxide (CNO; Tocris, 6329, 0.05 mg/kg) in the central dorsal aspect of the auricular skin once per day on days 0–3. CNO administration was completed 1 hr before intranasal *A. alternata* challenge. Mice were lightly anesthetized with 3.5% isoflurane during the procedure.

For lineage-restricted activation in the auricular skin, TRPV1-hM3Dq or R26-LSL-Gq-DREADD (Control-hM3Dq) mice received i.d. CNO as described above. For VG-restricted activation, *Trpv1*^{Cre} mice first received an intraganglionic injection of AAV9-hSyn-DIO-hM3Dq-mCherry (AAV-DIO-hM3Dq-mCh; Addgene, #44361-AAV9, $\geq$10 ^12 vg/mL, 0.5 μL per ganglion) or AAV9-hSyn-DIO-mCherry (AAV-DIO-mCh; Addgene, #50459-AAV9, $\geq$10 ^12 vg/mL, 0.5 μL per ganglion) as described above, then received i.d. CNO 3 weeks after viral injection.

For lineage-restricted silencing in the auricular skin, TRPV1-hM4Di or R26-LSL-Gi-DREADD (Control-hM4Di) mice received i.d. CNO as described above. For VG-restricted silencing, *Trpv1*^{Cre} mice received an intraganglionic injection of AAV9-hSyn-DIO-hM4Di-mCherry (AAV-DIO-hM4Di-mCh; Addgene, #44362-AAV9, $\geq$10 ^12 vg/mL, 0.5 μL per ganglion) or AAV-DIO-mCh as described above, then received i.d. CNO 3 weeks after viral injection.

VG-specific deletion of Calcb

To delete *Calcb* in VG neurons, *Calcb*$^{fl/fl}$ mice received bilateral intraganglionic injections of pENN-AAV9-hSyn-Cre-hGH (AAV-Cre; Addgene, #105555-AAV9, ≥10 ^12 vg/mL, 0.5 μL per ganglion) or AAV9-hSyn-mCherry (AAV-Control; Addgene, #114472-AAV9, ≥10 ^12 vg/mL, 0.5 μL per ganglion) using the same intraganglionic injection procedure described above. Mice were allowed to recover for 3 weeks after injection prior to experimentation.

Optogenetic activation of TRPV1$^+$ neurons

Trpv1^{Cre} mice received an intraganglionic injection with AAV9-hSyn-DIO-hChR2 (H134R)-EGFP-WPRE-hGH polyA (AAV-DIO-hChR2; BrainVTA, PT-4358, ≥10 ^12 vg/mL, 0.5 μL per ganglion) or AAV-DIO-mCh. Three weeks post-injection, mice were anesthetized with 2% isoflurane, and localized blue light was delivered to the conchal region of the auricle on days 0–3. Optical stimulation used a 473 nm 100 mW diode pumped solid-state laser (Laser Glow Technologies, Toronto, Canada), following a slightly modified protocol.[10] In brief, an optical cannula was positioned 1 cm from the conchal surface of the auricle. Stimulation was at a frequency of 10 Hz, pulse width of 10 ms, and a 10 sec on 5 sec off sequence for 30 min with a power density of 7.2 mW/mm^2. Mice underwent four 30-min stimulation sessions with at least 2 hrs between each session. The final optical stimulation session was completed 1 hr before intranasal *A. alternata* challenge.

CGRP receptor antagonist treatment

BIBN4096 (MedChemExpress, HY-10095) was dissolved in PBS. *Wild-type* mice received i.p. injection of BIBN4096 (1 mg/kg) or vehicle once daily on days 0–3, 30 min prior to auricular RTX or vehicle treatment on day 0, and 1 hr prior to intranasal *A. alternata* challenge on days 1–3.

Adrenergic fiber denervation

6-hydroxydopamine (6-OHDA; Sigma, H4381) was dissolved in 0.1% Ascorbic Acid (Sigma, PHR1008) in PBS. *Wild-type* mice received i.p. injection of 6-OHDA (0.2 g/kg) or vehicle once on day −5 prior to intranasal *A. alternata* challenge.

Muscarinic receptor blockade

Glycopyrrolate (Sigma, SML0029) was dissolved in PBS. *Wild-type* mice received i.p. injection of glycopyrrolate (2 mg/kg) or vehicle once daily on days 0–3, 30 min prior to auricular RTX or vehicle treatment on day 0, and 1 hr prior to intranasal *A. alternata* challenge on days 1–3.

Nicotinic receptor blockade

Mecamylamine hydrochloride (Sigma, M9020) was dissolved in PBS. *Wild-type* mice received i.p. injection of mecamylamine hydrochloride (5 mg/kg) or vehicle once daily on days 0–3, 30 min prior to auricular RTX or vehicle treatment on day 0, and 1 hr prior to intranasal *A. alternata* challenge on days 1–3.

Tracing of VG, DRG and auricular skin

For retrograde tracing from the auricular skin to the VG, AAV2-retro-Cre (VectorBuilder, VB220605-1075ztp, ≥10 ^12 vg/mL, 10 μL) was injected i.d. in the central dorsal aspect of the auricular skin of Ai9 mice. Three weeks after injection, VG, DRG, and TG were harvested and examined for tdTomato$^+$ neurons.

For viral-mediated anterograde tracing from the VG to the auricular skin, Ai9 mice received an intraganglionic injection of pENN-AAV9-hSyn-Cre-hGH (AAV-Cre; Addgene, #105555-AAV9, ≥10 ^12 vg/mL, 0.5 μL per ganglion). Three weeks after injection, the auricular and cheek skin were imaged for tdTomato$^+$ fibers.

For WGA-mediated anterograde tracing from VG, *wild-type* mice received an intraganglionic injection of WGA-AF647 (Thermo Fisher Scientific, W32466, 2 μg/0.5 μL per ganglion). Four days after injection, the auricular skin was harvested and underwent tissue clearing and whole-mount immunostaining.

For CTB-mediated retrograde tracing, *wild-type* mice received an i.d. injection of CTB-AF488 (Thermo Fisher Scientific, C34775, 5 μg) or intranasal CTB-AF647 (Thermo Fisher Scientific, C34778, 5 μg) on day 0. VG were harvested on day 4 for imaging.

For WGA-mediated anterograde tracing from DRG to the auricular skin, *wild-type* mice received intrathecal injection of WGA-AF488 (Thermo Fisher Scientific, W11261, 5 μg) in the L4-5 region. Four days after injection, the auricular skin was harvested and underwent tissue clearing and whole-mount immunostaining.

Tissue clearing and whole-mount staining

For VG, DRG, and TG samples, tissues were harvested from experimental mice and fixed in 4% paraformaldehyde (pH 7.4) overnight. Fixed tissues were washed with PBS, placed directly on slides, and covered with refractive index matching solution (RIMS: 40 g Histodenz (Millipore Sigma), 30 mL of 0.02M phosphate buffer, 0.1% Tween-20 (Millipore Sigma), and 0.01% sodium azide). After mounting, samples were equilibrated in RIMS overnight at room temperature in a humid chamber. Whole-mount ganglia were imaged in RIMS on a confocal microscope.

For skin tissue, hair was removed with depilatory cream and the skin was dissected from underlying tissue. Auricular skin was split into dorsal and ventral halves, and cartilage was removed with a scalpel. For cheek skin, subcutaneous fat was gently trimmed with a

scalpel. Tissues were then fixed in 4% paraformaldehyde at 4°C overnight, washed in PBS, then incubated overnight in PBS containing 0.05% sodium azide with gentle rotation. Clearing reagent (CUBIC-R1) was prepared by dissolving Quadrol (156 g, 80 wt%), urea (122 g), and distilled H_2O (144 g), followed by the addition of Triton X-100 (75 g) at RT with gentle mixing. Samples were incubated in CUBIC-R1 with 0.1% sodium azide at 37°C for 7 days with continuous gentle rotation. The reagent was replaced every 1–3 days. Cleared tissues were washed in PBS, blocked overnight in PBS-Blocking Buffer (PBS-BB: 1% BSA, 0.2% skim milk, 0.3% Triton X-100 in PBS) containing 0.1% sodium azide at 37°C, and incubated with a rabbit anti-CGRP antibody (BMA Biomedicals, T-4032, 1:300) diluted in PBS-BB containing 0.1% sodium azide for 3–4 days at RT with gentle rotation. After washing in PBS-Tr (0.3% Triton X-100 in PBS), tissues were incubated with a donkey anti-rabbit Alexa Fluor 594 secondary antibody (Thermo Fisher Scientific, A-21207, 1:500) in PBS-BB containing 0.1% sodium azide for 2 days at RT, washed again in PBS-Tr, and equilibrated in RIMS at RT for 2–3 days with rotation. For mounting, skin samples were placed directly on slides in RIMS and coverslipped. All images were captured using a Leica Stellaris8 confocal microscope. Image processing was performed in Fiji/ImageJ with identical parameters applied across conditions.

Immunohistochemistry

VG samples were fixed in 4% paraformaldehyde for 2 hrs on ice, washed with PBS, and incubated with 30% sucrose at 4°C overnight. Samples were then embedded in optimal cutting temperature (OCT) compound, snap-frozen, and cut into serial 14 μm sections. For blocking and permeabilization, sections were incubated for 45 min at RT in blocking buffer (1% BSA, 10% normal donkey serum, and 0.3% Triton X-100 in PBS). Anti-ATF3 antibody (Novus biologicals, NBP1-85816, 1:500) was diluted in blocking buffer and applied overnight at 4°C. After washing in PBST (0.2% Tween-20 in PBS; 3 × 10 min), sections were incubated for 1 hr at RT with a donkey anti-rabbit Alexa Fluor 594 secondary antibody (Thermo Fisher Scientific, A-21207, 1:500). After a final wash in PBST, sections were mounted in ProLong Gold Antifade Mountant with DAPI (Thermo Fisher Scientific, P36931). All images were captured using a Leica confocal microscope (Stellaris8).

VG neuronal culture and Ca^{2+} imaging

VG were harvested from Pirt-GCaMP3 mice and placed in 1 mL Ca^{2+}/Mg^{2+}-free Hank's Balanced Salt Solution (HBSS, Sigma-Aldrich) containing 40 units papain (Worthington Biochemical), 0.5 mM EDTA (Invitrogen) and 1.5 mM $CaCl_2$ (Research Products International) for 25 min at 37°C. VG were further dissociated in 1 mL of HBSS with 1 mg/mL collagenase type-1 (Worthington Biochemical) and 5 mg/mL dispase (Gibco) for 30 min at 37°C. Dissociated VG were gently triturated, pelleted, and resuspended in Neurobasal Plus Medium supplemented with 1% B-27 supplement (Gibco), Antibiotic-Antimycotic (Gibco, 100 U/mL penicillin, 100 μg/mL streptomycin, and 25 ng/mL Amphotericin B), 50 ng/mL mouse nerve growth factor (NGF, Gibco, #13257-019), and 10% heat-inactivated fetal bovine serum (Cytiva). After plating on an ibiTreat (tissue culture-treated) μ-Slide 8 well high chamber with #1.5 polymer coverslip (Ibidi), VG neurons were cultured in a humidified incubator at 37°C for 3 days before use.

Before Ca^{2+} imaging experiments, neuronal cultures were washed 3 times and placed in artificial cerebrospinal fluid (ACSF: 125 mM NaCl, 5 mM KCl, 2 mM $CaCl_2$, 2 mM $MgCl_2$, 25 mM D-Glucose, and 10 mM HEPES with pH adjustment to 7.4 by NaOH) for 30 min. During the recording, fluorescence was recorded at an excitation wavelength of 510 nm using an inverted Zeiss Axio Observer 8 controlled by Zen Blue software (Zeiss) equipped with a live-cell chamber capable of maintaining a temperature of 37°C and 5% CO_2 environment. Neurons were stimulated with vehicle (ACSF), followed by *A. alternata* protein extract (10 μg/mL) and high potassium solution (140 mM KCl, 5 mM NaCl, 2 mM $CaCl_2$, 2 mM $MgCl_2$, 25 mM D-Glucose, and 10 mM HEPES with pH adjustment to 7.4 by NaOH). A neuronal response was defined as an increase in fluorescence of > 15% above baseline. Only neurons responding to KCl were considered viable and included in downstream analyses. Ca^{2+} responses are presented as $\Delta F/F0$, where F0 is the baseline fluorescence and F is the peak fluorescence.

Flow cytometry

Single-cell suspensions were prepared as previously described.[3] Three lobes of the right lung were placed in 5 mL HBSS containing Liberase TM (Roche, 5401119001, 50 μg/mL) and DNase I (Roche, 4536282001, 40 μg/mL) in a gentleMACS C-tube (Miltenyi Biotec), dissociated using the "37_m_LDK1" program on a gentleMACS Dissociator with Heaters (Miltenyi Biotec), passed through a 70 μm cell strainer (Fisher Scientific), washed with PBS containing 2% FBS, and centrifuged (400 g, 5 min, 4°C). Pelleted cells were incubated with 1 mL red blood cell lysing buffer (MilliporeSigma) at RT for 1 min, then washed and resuspended in 2% FBS/PBS. Samples were stained with a Zombie NIR viability dye (BioLegend, 423105, 1:500) according to the manufacturer's instructions. Nonspecific antibody binding was blocked with an anti-CD16/32 antibody (Bio X Cell, BE0307, 1:100), followed by staining for surface antigens (Key resources table). For intracellular staining of IL-5 and IL-13, cells were resuspended in complete RPMI (RPMI 1640 supplemented with 10% FBS, 1% penicillin-streptomycin, 2 mM L-glutamine, 1 mM sodium pyruvate, 10 mM HEPES, and 50 μM 2-mercaptoethanol) and stimulated for 4 hrs with phorbol 12-myristate 13-acetate (Sigma, P1585, 0.5 μg/mL) and ionomycin (Invitrogen, I24222, 4 μg/mL) in the presence of brefeldin A (BioLegend, 420601) and monensin (BioLegend, 420701). Cells were then washed, surface-stained, fixed/permeabilized, and stained intracellularly. ILC2s were identified within the lymphocyte gate as live $CD45^+$ Lin^- $CD90^+$ $CD127^+$ Sca-1^+ KLRG-1^+ cells (Lin: CD3, CD4, CD8, CD11b, CD11c, and B220). Eosinophils were identified as live $CD45^+$ Siglec F^+ $CD11c^-$ cells. Samples were acquired on a Cytek Aurora flow cytometer (Cytek). Data were analyzed using FlowJo 10 and GraphPad Prism 9.0.

ELISA

BALF was collected by 1 mL PBS lavage. Protein levels of IL-5, IL-13, Substance P, CGRPα, and CGRPβ in BALF were measured by ELISA kits according to the respective manufacturers' instructions (IL-5: Mouse IL-5 Duo Set ELISA Kit, R&D, DY405; IL-13: Mouse IL-13 Duo Set ELISA, R&D, DY413; Substance P: Substance P ELISA kit, Enzo, ADI-900-018A; CGRPα: Mouse CGRP1 ELISA Kit, MyBioSource, MBS2509891; CGRPβ: Mouse CGRP2 ELISA Kit, MyBioSource, MBS7241942).

Real-time qPCR

Mouse VG were harvested and homogenized with Sonic Dismembrator (Thermo Fisher Scientific, FB120110) in lysis buffer RLT (-QIAGEN, 79216). Total RNA was extracted with the RNeasy Plus Micro Kit (QIAGEN, 74034) following the manufacturer's protocol. Equal amounts of cDNA were synthesized from RNA extracts using QuantiTect Reverse Transcription Kit (QIAGEN, 205311). Gene expression levels were measured using TaqMan Gene Expression Assays (Key resources table: *Calcb*, Mm00446495_m1 and *Gapdh*, Mm99999915_g1) and TaqMan Fast Advanced Master Mix (Thermo Fisher Scientific, 4444556). Reactions were cycled using the Applied Biosystems QuantStudio6 Pro Real-Time PCR Systems (Thermo Fisher Scientific) using the manufacturer's protocol. Gene expression was normalized to *Gapdh*, and relative expression was calculated using the ΔΔCt method.

QUANTIFICATION AND STATISTICAL ANALYSIS

Statistical analyses were performed using GraphPad Prism 9.0 software. Data are presented as mean ± SEM. Group comparisons were done using unpaired t-tests with Welch's correction or a two-way ANOVA with multiple comparison tests as indicated in figure legends.